Surface Science 617 (2013) 175–182

Contents lists available at ScienceDirect

Surface Science

journal homepage: www.elsevier.com/locate/susc

Structure and stability of acrolein and allyl alcohol networks on Ag(111) from density functional theory based calculations with dispersion corrections

Ricardo M. Ferullo [a], Maria Marta Branda [b], Francesc Illas [c,*]

[a] INQUISUR, Departamento de Química, Universidad Nacional del Sur, Bahía Blanca, Argentina
[b] IFISUR, Departamento de Física, Universidad Nacional del Sur, Bahía Blanca, Argentina
[c] Departament de Química Física and Institut de Química Teòrica i Computacional (IQTCUB), Universitat de Barcelona, C/Martí i Franquès 1, E-08028 Barcelona, Spain

ARTICLE INFO

Article history:
Received 3 May 2013
Accepted 4 July 2013
Available online 13 July 2013

Keywords:
Acrolein
Allyl alcohol
Ag(111)
Ordered overlayers
DFT-D

ABSTRACT

The interaction of acrolein and allyl alcohol with the Ag(111) surface has been studied by means of periodic density functional theory based calculations including explicitly dispersion terms. Different coverage values have been explored going from isolated adsorbed molecules to isolated dimers, interacting dimers or ordered overlayers. The inclusion of the dispersion terms largely affects the calculated values of the adsorption energy and also the distance between adsorbed molecule and the metallic surface but much less the adsorbate–adsorbate interactions. Owing to the large dipole moment of acrolein, the present calculations predict that at high coverage this molecule forms a stable extensive two-dimensional network on the surface, caused by the alignment of the adsorbate dipoles. For the case of allyl alcohol, dimers and complex networks exhibit similar stability.

1. Introduction

Competitive adsorbate–adsorbate and adsorbate–substrate interactions at surfaces are responsible for the formation of different superstructure patterns, from highly ordered self-assembled structures to complex disordered ones. The adopted molecular geometry and the activation of chemical bonds present in these surface arrays are critical aspects which are in direct relation with possible applications in nanotechnology as well as with the catalytic activity and selectivity of the resulting systems. Precisely, a relationship between coverage, molecular orientation and selectivity was recently proposed for the hydrogenation of acrolein (propenal). This simple aldehyde is often chosen as a prototype for the study of the chemoselective hydrogenation of α,β-unsaturated aldehydes to the corresponding unsaturated alcohols, widely used as pharmaceutical precursors and in the fragrance industry [1,2]. Suitable catalysts must be used for this reaction because thermodynamics favors the hydrogenation of the C=C bond. Experiments using high resolution synchrotron X-Ray Photoelectron Spectroscopy (XPS), Near Edge X-Ray Absorption Fine Structure (NEXAFS) and Temperature Programmed Desorption (TPD) have shown that the structure of acrolein adsorbed on Ag(111) strongly depends on the coverage and that at high coverage the structure has the C=C bond markedly tilted away from the surface [3]. From this experimental study, the structure proposed for the adsorbed acrolein at high coverage has the C=O bond almost parallel (2°) to the surface but the C=C bond is tilted by 12°. This change of orientation with coverage is claimed to be responsible for the observed chemoselectivity. On the other hand, the same authors pointed out that, on the same surface, the desired product, the allyl alcohol, has a C=C angle tilted about 30° when it is coadsorbed with hydrogen at low coverage (at 0.3 ML of hydrogen) and changes to only 3° at high hydrogen coverage, bringing the C=C bond nearly parallel to the surface. Thus, the preference for the production of allyl alcohol from adsorbed acrolein, which is observed to be more favored at low H coverage, has to be attributed to the geometric orientation of the C=C bond of the reactant which hinders, at least partially, the attack by H.

Very recently, Wei et al. have investigated the hydrogenation of acrolein on silica-supported silver catalysts with various particle sizes (1–9 nm) [4]. They found that the selectivity to allyl alcohol and turnover frequency increased with increasing particle size. As the authors have pointed out, the results appear as somewhat unusual because the most active catalyst is also the most selective. Increasing the total pressure from 1 to 5 atm was also found to increase the selectivity and decrease the activation energy. These results also suggest that, on flat surfaces, a tilted orientation of acrolein, preferably at high coverage, is desirable for high selectivity and high activity.

In a previous work we have investigated the structure of acrolein adsorbed on Ag(111) using density functional theory (DFT) based calculation with the PW91 form of the Generalized Gradient Approach exchange-correlation potential [5]. Our calculations evidenced that, at low coverage, the preferred structure for adsorbed acrolein is parallel to the surface, in agreement with experiments. However, at higher

* Corresponding author. Tel.: +34 93 4021229; fax: +34 93 4021231.
E-mail address: francesc.illas@ub.edu (F. Illas).

0039-6028/$ – see front matter © 2013 Elsevier B.V. All rights reserved.
http://dx.doi.org/10.1016/j.susc.2013.07.005

coverage, we found that different complex networks are possible with different orientations with respect to the surface, which contrast with the above-mentioned NEXAFS results. Due to the fact that these experiments provide only average structural parameters, we concluded that the different calculated structures should be considered as input data to interpret NEXAFS experiments with similar coverage situations. Nevertheless, one must advert that our previous study neglected dispersion or van der Waals (vdW) interactions which have been found to play an important role in the adsorption geometry and energetics of adsorbed molecules, and intermolecular interactions as well [6–12]. This is because most of the commonly used DFT based methods rely on approximations of the electron exchange and correlation which do not properly describe the long-range vdW forces.

In the past few years, a considerable effort has been devoted to include vdW interactions in DFT based methods. The simplest approximation consists in employing an empirical correction, leading to the so-called DFT-D methods [13]. These are simply based on the addition of damped atom-pairwise dispersion corrections of the form C_6R^{-6}, where C_6 represents a dispersion coefficient for a given atom pair and R is the distance between the atoms. The implementations of Ortmann et al., [14] Grimme, [15] and Tkatchenko and Scheffler [16] constitute widely used representatives of DFT-D methods. On the other hand, approaches aimed at providing a first-principles description of vdW interactions have also been developed. These methods are usually referred to as vdW-DF and can be computationally more demanding. Among these, a promising approximation is the one proposed by Dion et al. [17] and other functionals obtained by modifications of this one resulting in different vdW-DFT flavors, such as the rPW86-vdW, [18] optPBE-vdW and optB88-vdW, [19] and optB86b-vdW [20] although their performance is still not fully established and, in absence of experimental data, it is really difficult to justify a given choice. This is clear from the recent review by Prates-Ramalho et al. [21] on the performance of different methods aimed to account for van der Waals interactions between adsorbates and surfaces in density functional theory based methods. In fact, very recent work for the interaction of graphene with Ni (111) has shown that among a rather long list of functionals proposed to include van der Waals interactions, only optB86b-vdW and the empirical DFT-D of Grimme are able to provide a balanced description of the experimentally well-established physisorption and chemisorption states, the attachment strength of the latter on the Ni(111) surface, the graphene–Ni(111) separation, and the band structure of chemisorbed graphene [22]. Hence, in spite of some claims, that Grimme's DFT-D method is too empiric, it still appears to be robust enough to distinguish the two states for graphene on Ni(111) and, also, the exfoliation energy of graphite [22].

In the present work we report DFT based calculations for low and high coverage of acrolein and allyl alchohol on Ag(111) which include dispersion corrections for vdW interactions mainly through DFT-D, which is justified by the above arguments regarding the case of graphene on Ni(111), with some calculations carried out also with optB86b-vdW mainly for comparison purposes. We have already mentioned that these unsaturated aldehydes and alcohols are of interest in selective hydrogenation processes [23–27] and that experimental information for the geometric structures of these molecules on Ag(111) is at hand; [3] which can be taken as a reference. Our main objective here is to study geometries and relative stabilities of acrolein and allyl alcohol networks on Ag(111) and the effect of the dispersion interaction on these systems.

1.1. Computational details

Periodic slabs consisting of four layers of metal atoms interleaved with a vacuum width equivalent to five atomic layers were employed to determine adsorption geometry of adsorbed acrolein (denoted as ACR) and allyl alcohol (denoted as AOL). For the low coverage case, a $p(4\times4)$ supercell is used while for the high coverage situation several structures are considered. The first one is represented by a $p(2\times2)$ cell which corresponds to a coverage four times larger than the one corresponding to the low coverage case modeled by the $p(4\times4)$ supercell. In this situation the adsorbed molecules are all equivalent and thus oriented in the same way (head-to-tail). Another possible structure arising from the interaction between adsorbed molecules involves a head-to-head type of contact and thus allows for the formation of dimers and more complex structures. To take into account these head-to-head interactions we use $p(5\times3)$ and $p(4\times2)$ cells containing explicitly two non-equivalent molecules initially placed in a head-to-head manner although the resulting structure is, in all cases, fully relaxed. Note, that in the $p(4\times2)$ cell with two adsorbed molecules the coverage is the same as in the $p(2\times2)$ cell with one adsorbate. However, in the former supercell different orientations of the two adsorbed molecule are possible whereas in the latter this is not the case because of the periodic symmetry. In the $p(5\times3)$ cell the coverage is such that the adsorbed molecules are also allowed to form dimers but rather separated from each other.

For each of the surface structures mentioned above, the energy was evaluated at DFT and DFT-D levels. Following our previous work devoted to ACR on Ag(111), [13] we used the PW91 exchange-correlation potential [28,29] version of the Generalized Gradient Approximation (GGA) for DFT based calculations without dispersion corrections. Since the empirical corrections to this GGA functional are not available, we used the DFT-D approximation suggested by Grimme using PBE [15]. Note, however, that the performance of PW91 and PBE is very similar even in the energy profile for surface reactions [30] and that, indeed, it has been very recently shown that these functionals provide the best overall performance for the bulk properties of the thirty transition metal elements [31]. In the DFT-D approach, the total energy is given by

$$E^{\mathrm{DFT-D}} = E^{\mathrm{DFT}} + E_{\mathrm{disp}}, \tag{1}$$

where E^{DFT} is the Kohn–Sham total energy as obtained from genuine PBE and E_{disp} is an empirical dispersion correction given by

$$E_{\mathrm{disp}} = -s_6\sum_{i,j} f\left(R_{ij}\right)C_6^{ij}\left(R_{ij}\right)^{-6}, \tag{2}$$

where $f(R_{ij})$ represents a damping function and the C_6^{ij} coefficients are obtained from atomic polarizabilities and ionization potentials. On the other hand, s_6 is a scaling factor which was optimized in 0.75 for PBE [15].

The one electron Kohn–Sham states were expanded in a plane wave basis with a kinetic cut off energy of 415 eV and the PAW method [32] was used to take into account the effect of the inner cores on the valence states. Suitable Monkhorst–Pack [33] meshes have been used to carry out all necessary integration steps in the reciprocal space. These are as follows: $5\times5\times1$ for the $p(2\times2)$ cell, $3\times3\times1$ for the $p(4\times4)$ cell, and $3\times5\times1$ for both $p(4\times2)$ and $p(5\times3)$ cells. The adsorbate-induced dipole moment in the vacuum region was eliminated following the method outlined by Kresse et al. [34] Both DFT and DFT-D periodic calculations were performed using the VASP code [35,36]. The adsorption energy (E_{ads}) was calculated with respect to the naked surface and to the gas phase molecule (the most stable conformer of ACR or AOL). In all cases, the structure of the adsorbed molecule(s) and the two topmost layer of the Ag(111) surface model have been fully relaxed; the other two metal layers were maintained fixed at the bulk geometry. This strategy is commonly used when studying the chemistry of metal surfaces, the case of ethylene partial oxidation on Ag(111) studied by different authors [37–40] provides a beautiful example of the appropriateness of this model which is also supported by low-energy electron diffraction studies which show slight relaxations of the first two interlayer distances with respect to the bulk distance, namely, −0.5% for Δd_{12} and −0.4% for Δd_{23}, and even smaller relaxation

between the third and fourth layers [41]. We observe similar results using DFT: −0.7% and −1.3% for Δd_{12} and Δd_{23}, respectively. The addition of the dispersion term shows a slight expansion of +1.3% for Δd_{12} and a contraction of −0.7% for Δd_{23}. Interestingly enough, optB86b predicts a slightly different behavior with a contraction of −2.6% for Δd_{12} and a larger contraction of −3.3% for Δd_{23}. Optimized geometries were found when the forces on atoms were smaller than 0.01 eV/Å.

To further test the reliability of the DFT-D approach chosen in this work we have performed additional calculations for the adsorption on Ag(111) of two closely related molecules such as formaldehyde and methanol for which experimental values for the adsorption energy, mainly from thermal programmed desorption experiments exist [42,43]. The experimental values and calculations carried out using the present computational setup are reported in Table 1. The calculations have been carried out using the $p(4 \times 4)$ supercell to avoid lateral interactions. From the results in Table 1 it is clear that not surprisingly, the DFT values for the adsorption energy are largely underestimated with the rather small calculated value likely being due to self-interactions effects. On the other hand, DFT-D appears to slightly overestimate the adsorption energy values, although the results are nonetheless in good agreement with that of experiments. In particular it is interesting to highlight the fact that the difference between the experimental adsorption energies of formaldehyde and methanol is essentially the same predicted by the DFT-D calculations (~0.15 eV). Moreover, the DFT-D predicted distance between the molecule and the surface (d_{Ag-O}) is about 0.08 Å shorter than the value predicted by DFT, as expected. Note also that the present results for the adsorption of formaldehyde on Ag(111) are essentially the same as those reported by Reckien et al. [11] using a similar DFT-D parametrization.

2. Results and discussion

2.1. Adsorbed acrolein

In the present study only the more stable conformer of ACR has been considered (s-trans) and the optimized geometries for the different situations described in the previous section are displayed in Figs. 1 and 2. Let us first consider the effect of the dispersion term in the adsorption of ACR by comparing results from DFT and DFT-D. In the case of the $p(4 \times 4)$ supercell representing the low coverage regime calculations have also been carried out using the, in principle more refined, optB86b approach. From the results in Table 2 it is clear that both DFT-D and optB86b predict larger values for E_{ads} (0.61 and 0.45 eV, respectively) than PBE which predicts an almost negligible interaction (0.06 eV). Note also that the somewhat larger value predicted by the DFT-D methods is in line with the well-known trend of this approach to overestimate van der Waals interactions. However, it is also worth pointing out that the structure of the adsorbed molecule predicted by DFT-D and optB86b is quite different, the latter being indeed in disagreement with experiments as further commented on below.

Regarding the rest of situations one may observe that in some cases, the distance from the adsorbate to the surface, measured from distance between the O atoms and the nearest Ag atom, decreases dramatically by about 1 Å (Table 2). Interestingly, both DFT and DFT-D predict the $p(2 \times 2)$ superstructure as the most stable one. However, the difference between DFT and DFT-D calculated adsorption energy values is significantly large and the relative stability of the $p(2 \times 2)$ superstructure is also more pronounced at the DFT-D level. This is because, in this superstructure, the adsorbed molecules form a compact network in which each molecule interacts with four nearest neighbors through four O – H contacts (two on the tail and two on the head). Concerning the intramolecular geometrical parameters, both the C═C and C═O distances are slightly larger at the DFT-D level fundamentally due to the enhancement of the adsorbate–substrate attractive interaction (see below). This is in agreement with a decrease in the DFT-D calculated vibrational frequency of the C═C and C═O stretching which are about 70 and 40 cm^{-1}, respectively, smaller than the DFT values. At this high coverage the angle between the C═O bond and the perfect surface plane angle (θ) is 2.5 and 7.1° using DFT and DFT-D, respectively, in both cases tilted away from the surface, i.e., with the C═O bond pointing upward moving away from the surface. However, at the very low coverage represented by the $p(4 \times 4)$ supercell, the θ angle predicted by DFT is 4.9° towards the surface and it changes to 8.2° but tilted away from the surface when including dispersion terms through the DFT-D method. This is quite close to the value estimated from NEXAFS measurements; θ = 2° at low ACR coverage. The agreement is not quantitative but shows that both DFT and DFT-D tend to place the molecule almost parallel to the surface. This is not the case when using the, in principle more refined, optB86b method since it predicts a much larger value for the θ angle (Table 2). Accordingly, only DFT-D results are described in the following discussion . On the other hand, for the situation represented by the (4×2) regime (head-to-head orientation) and starting from a structure with both ACR molecules parallel to the surface only a structure is found with pure DFT in which the molecular network involves chains of adsorbed ACR molecules in a zig-zag manner in such a way that each molecule interacts with two nearest neighbors through O – H contacts (Fig. 1d). In this structure one molecule is almost parallel and one almost perpendicular to the surface. Conversely, with DFT-D, apart from obtaining a similar superstructure (referred hereafter as structure I), we have found a second array (labeled as structure II) with essentially the same adsorption energy and with the geometry presented in Fig. 1e, in which one of the C═O bonds is tilted by about 25°with respect to the surface.

Let us now discuss the results predicted by the DFT-D calculations in some more detail and focusing on the different overlayers which are formed at different coverages. It has already been mentioned that for the coverage situation represented by the $p(2 \times 2)$ supercell, a compact and stable superstructure is formed. In this adsorbed overlayer, the C═C and C═O bond distances are 0.04 and 0.02 Å, respectively, longer than those corresponding to the free, gas phase, ACR molecule with a concomitant red shift of the corresponding stretching vibrational frequencies by about 130 and 120 cm^{-1} with respect to the values predicted for the free molecule using the same computational method (Table 2). It is worth pointing out that these structural changes with respect to the isolated ACR molecule are considerably more important than those predicted for the other structures considered in the present work and one is tempted to take these changes as indicative of some activation of these bonds. The tendency to form ACR dimers can be further evaluated by inspecting the changes in the energetic stability of the adsorbed molecule in going from the $p(4 \times 4)$ supercell, where the adsorbed ACR molecules are isolated, to the situation represented by the $p(5 \times 3)$ supercell, where the adsorbed molecules are allowed to exhibit head-to-head interactions and thus form well defined and isolated ACR dimers. In this latter situation an increase of only 0.05 eV per molecule indicates a slight tendency to form dimers which is even smaller than that for free ACR where the energy gained upon dimer formation is 0.09 eV per molecule. Comparing these results with

Table 1
Adsorption energy values for formaldehyde (H_2CO) and methanol (CH_3OH) on Ag(111) as obtained from DFT (PW91), DFT-D (PBE-D) calculation and from thermal desorption (TD) measurements.

		E_{ads} (eV)	d_{Ag-O}
H_2CO	DFT	0.08	2.813
	DFT-D	0.34	2.739
	TD[42]	0.27	–
CH_3OH	DFT	0.14	2.637
	DFT-D	0.49	2.547
	TD[43]	0.41	–

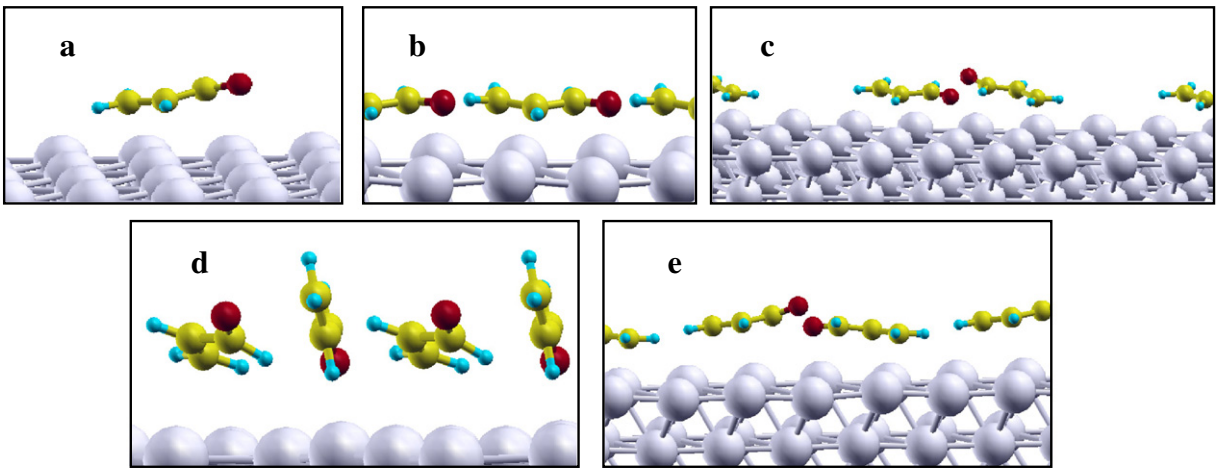

Fig. 1. Side views of the DFT-D optimized geometry of adsorbed acrolein on Ag(111) corresponding to a) $p(4 \times 4)$; b) $p(2 \times 2)$; c) $p(5 \times 3)$; d) $p(4 \times 2)$ (structure I); e) $p(4 \times 2)$ (structure II).

those obtained for the two higher coverage situations represented by the $p(2 \times 2)$ and $p(4 \times 2)$ supercells it clearly appears that the head-to-tail orientation is preferred to the head-to-head one. Taking into account the large dipole moment of ACR – 3.11 ± 0.04 D from experiments [44] and 3.72 D according to the present DFT based calculations – the higher stability of the head-to-tail array can be understood as caused by the alignment of the adsorbate dipoles which form an extensive two-dimensional network on the surface. The present situation is reminiscent of that encountered for HF adsorption on Au(111) [45] where an increased stability with increasing coverage was observed and attributed to the formation of a compact two-dimensional H-bonded array resulting from the rather large dipole moment of HF ($\mu = 1.98$ D). On the other hand, the fact that the results corresponding to the $p(5 \times 3)$ and $p(4 \times 2)$ unit cells are so similar with adsorption energy values of 0.66 and 0.63 eV per molecule, respectively, indicates a very weak repulsion interaction among the formed surface dimers.

2.2. Adsorbed allyl alcohol

The isolated allyl alcohol (AOL) molecule exhibits five different conformers and, hence, the modeling of AOL adsorption is considerably more complex than that of ACR, especially because of the larger number of molecular networks at the surface to consider. The conformers are designated according to the usual notation which refers to the relative position of the hydroxyl group (C = cis or G = gauche) to the carbon=carbon double bond (rotation around the C–C bond) and to the orientation of the hydroxyl group (rotation around the C–O bond; t = trans, g or g′ = gauche). In this way, the five conformers can be indicated as Gg, Gt, Gg′, Cg and Ct. From temperature dependent infrared spectra and ab initio (MP2 and B3LYP) calculations it was established that the Gg conformer is the most stable gas phase structure with an estimated abundance of about 54% at room temperature [46]. In agreement with the findings of Durig et al. [46] just commented on, we found that the Gg conformer is predicted to be the most stable

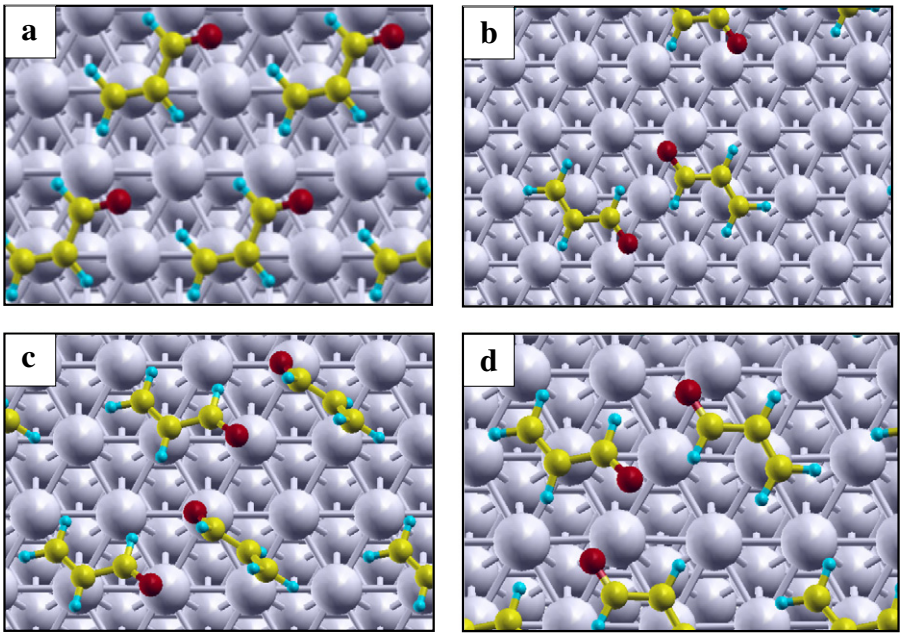

Fig. 2. Top views of the DFT-D optimized geometry of the network of adsorbed acrolein on Ag(111) corresponding to a) $p(2 \times 2)$; b) $p(5 \times 3)$; c) $p(4 \times 2)$ (structure I); d) $p(4 \times 2)$ (structure II).

Table 2
Bond lengths (Å), bond angles (degrees), vibrational frequencies (cm^{-1}) and adsorption energies (eV) of acrolein on the Ag(111) surface. The θ angle is defined by the C═O bond and the perfect unrelaxed surface plane. Adsorption energies are calculated as the average per adsorbed molecule.

	Method	$d_{C=C}$	$d_{C=O}$	d_{Ag-O}	$\nu_{C=C}$	$\nu_{C=O}$	∠C═CH_2	θ	E_{ads}
Gas phase	DFT	1.340	1.224	–	1617	1708	–	–	–
	DFT-D	1.341	1.225	–	1621	1711	–	–	–
p(4 × 4)-ACR	DFT	1.342	1.227	3.560	1619	1695	0.7[a]	4.9[b]	0.06
	DFT-D	1.365	1.232	3.126	1529	1643	3.4[b]	8.2[a]	0.61
	optB86b	1.343	1.234	2.677	–	–	33.3[a]	36.4[b]	0.45
p(2 × 2)-ACR	DFT	1.344	1.232	4.222	1608	1677	4.4[b]	2.5[a]	0.17
	DFT-D	1.381	1.245	3.221	1493	1593	2.0[b]	7.1[a]	0.89
p(5 × 3)-2ACR	DFT	1.342	1.230	4.176	1623	1692	5.0[b]	2.4[a]	0.10
		1.342	1.231	3.547	1620	1674	5.4[a]	9.2[b]	0.66
	DFT-D	1.355	1.236	3.135	1563	1642	2.2[b]	3.1[a]	
		1.363	1.237	3.185	1536	1625	2.7[b]	7.5[a]	
p(4 × 2)-2ACR (I)	DFT	1.342	1.229	4.935	1615	1686	29.4[b]	30.3[a]	0.15
		1.341	1.232	2.724	1626	1675	57.4[a]	54.1[b]	0.62
(I)	DFT-D	1.352	1.234	3.862	1622	1714	18.6[b]	27.9[a]	0.63
		1.341	1.237	2.503	1569	1649	50.5[a]	47.2[b]	
(II)	DFT-D	1.351	1.230	4.145	1572	1670	13.9[b]	25.1[a]	
		1.374	1.248	2.664	1508	1548	2.0[a]	9.4[b]	

[a] Tilted away from the surface.
[b] Tilted towards the surface.

one. Nevertheless, we have also investigated the overlayer structures that can be formed by the adsorbed Gt and Gg′ conformers. Note that even when considering the G-conformers only, the number of possible orientations of the AOL molecule on Ag(111) is still very large since the AOL molecule can be oriented with the C═C bond parallel or tilted to the surface. Furthermore, for each of these structures, the OH group can be oriented in different ways by rotating with respect to the C–O bond. Therefore, we carried out an initial study of adsorption by testing different orientations and using the $p(4 \times 4)$ supercell at DFT-D level; some of the studied structures are presented in Fig. 3 (cases d to f). The most stable structure resulted to be that with the C═C parallel to the surface and with the OH group oriented to the surface as in Fig. 3d (see also Fig. 4a). The calculated E_{ads} is 0.77 eV and corresponds to the Gt conformer thus indicating a change in the order of stability as compared with the gas phase values. For the adsorbed Gg conformer but with the C═C bond tilted with respect to the Ag(111) surface, the corresponding calculated E_{ads} is close (0.59 eV); still a different but energetically close situation is encountered for this Gg conformer ($E_{ads} = 0.62$ eV) when the OH group is tilted away from the surface. The complexity of the system is further illustrated by the structure of the Gg conformer with the C═C bond parallel to the surface but with the H belonging to OH pointing directly the surface (not shown in the figures) for which $E_{ads} = 0.70$ eV.

To simplify the discussion and in agreement with the results commented above for the $p(4 \times 4)$ supercell, in the following we consider only the geometries with the C═C parallel to the surface but allowing the rotation of OH around the C–O bond. In order to investigate the possible ordered overlayers we consider the same supercells used to study the structures of adsorbed ACR at various coverages; the calculated values are presented in Table 3 and include pure DFT calculations for comparison whereas the optimized structures are schematically displayed in Fig. 4. From the structural data collected in Table 3 it is clear that the effect of dispersion terms on the distances is smaller than that in the case of ACR. However, as for ACR, upon introduction of dispersion terms the adsorption energy values undergo a substantial increase.

For the coverage represented by the $p(2 \times 2)$ structure forcing a head-to-tail orientation, the AOL molecules do not tend to form dimers through the formation of H-bonds. In fact, starting from a structure in which the O–H is nearly parallel to the surface we obtained the geometry presented in Figs. 4b and 5a with the O–H bond directly pointing to the surface (Gg conformer). The adsorption

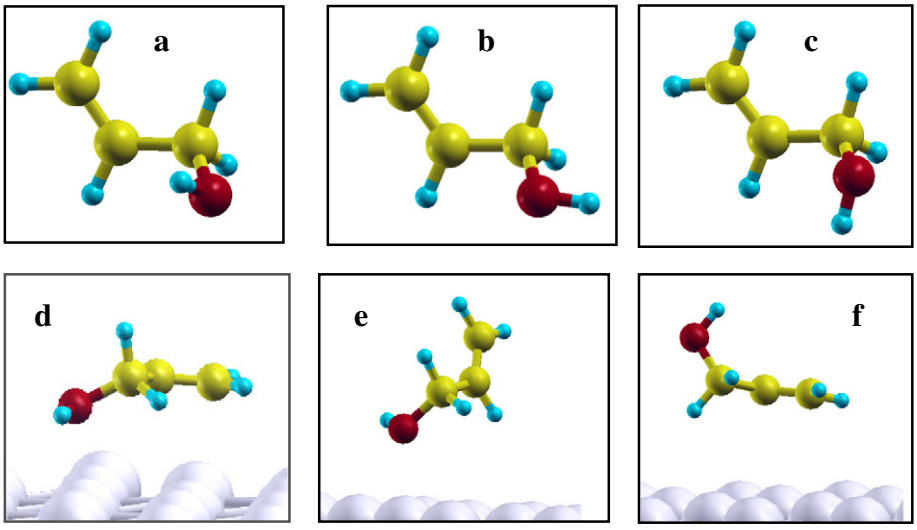

Fig. 3. Molecular structure of the Gg (a), Gt (b) and Gg′ (c) conformers of the isolated allyl alcohol and three different orientations (d, e and f) of adsorbed allyl alcohol as predicted from the DFT-D calculations carried out using the $p(4 \times 4)$ supercell.

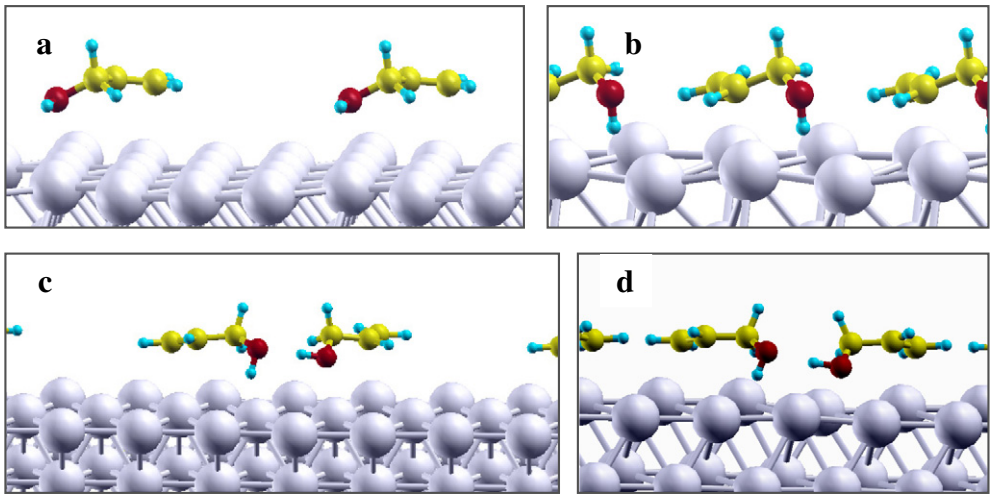

Fig. 4. Side views of the DFT-D optimized geometry of adsorbed allyl alcohol on Ag(111) corresponding to a) $p(4 \times 4)$; b) $p(2 \times 2)$; c) $p(5 \times 3)$ and d) $p(4 \times 2)$ supercells.

energy is 0.88 eV, very similar to the corresponding structure for ACR. However, when the molecules are oriented head-to-head the formations of dimers is favored as evidenced from the calculations using the $p(5 \times 3)$ and $p(4 \times 2)$ cells. The corresponding optimized structures are presented in Figs. 4c, d and 5 (right panel). These structures evidence the formation of H-bonds with one O–H bond nearly parallel to the surface and the other pointed to the surface in such a way that the resulting dimer can be viewed as a Gt–Gg pair. The tendency to form adsorbed dimers through head-to-head interactions can be deduced by comparing the E_{ads} for the $p(4 \times 4)$ and $p(5 \times 3)$ situations, 0.14 eV per molecule. This value is larger than the one corresponding to the formation of similar dimeric structures in the gas phase (0.08 eV per molecule). Furthermore, the agglomeration of dimers, observed by passing from $p(5 \times 3)$ to $p(4 \times 2)$ ($E_{ads} = 0.91$ and 0.89 eV per molecule, respectively), and similarly for the same situation for ACR, indicate only a very weak repulsion interaction among the formed surface dimers. Contrarily to the situation for adsorbed ACR, the two situations representing high coverages – $p(2\times2)$ and $p(4\times2)$ – exhibit essentially the same E_{ads} values, a clear indication that there is no preference for a particular orientation of the adsorbed oriented molecules. This situation is also different from that reported for ACR, because AOL presents a smaller dipole moment (1.55 ± 0.04 D [47]; 1.67 D from DFT) and hence the tendency to form stable aligned dimers (head-to-tail) is not as strong in relation to the array with interacting dimers (head-to-head).

2.3. Analysis of the interactions

The E_{ads} values reported in Tables 2 and 3 can be separated in two terms, one due to adsorbate–surface interactions (E_{s-a}) and the other due to intermolecular adsorbate–adsorbate interactions (E_{a-a}). In the present work E_{s-a} is defined as the interaction energy of the adsorbed molecular layer per molecule with respect to the isolated network with the geometry fixed at the one corresponding to the adsorbed overlayer but without the metallic slab surface model beneath it. In a similar way, the E_{a-a} term is calculated as the difference per molecule between the energy of the unsupported overlayer and that of the isolated gas phase molecule. The E_{s-a} and E_{a-a} values for the adsorption of both ACR and AOL are presented in Table 4 for pure DFT and DFT-D.

In all cases it is clear that the dispersion term affects very strongly the adsorbate–substrate interaction energy but much less the adsorbate–adsorbate contribution. For the high coverage regime of ACR represented by the $p(2 \times 2)$ supercell, which is the energetically preferred structure, both the E_{a-s} and the E_{a-a} contributions are the largest among all the situations of ACR adsorption. For this structure, it is interesting to note that the E_{a-a} term is essentially the same using DFT or DFT-D indicating the electrostatic nature of this interaction which is already well represented by the PW91 exchange-correlation potential. Another interesting point concerns the two different structures found within the $p(4 \times 2)$ supercell; both cases exhibit

Table 3
Bond lengths (Å), bond angles (degrees), vibrational frequencies (cm^{-1}) and adsorption energies (eV) of allyl alcohol (AOL) on the Ag(111) surface. Adsorption energies are calculated as the average per adsorbed molecule.

Supercell	Method	$d_{C=C}$	d_{O-H}	d_{Ag-O}	$\nu_{C=C}$	ν_{O-H}	$\angle C{=}CH_2$	E_{ads}
Gas phase	DFT	1.335	0.974	–	1650	3725	–	–
	DFT-D	1.337	0.974	–	1648	3713	–	–
$p(4 \times 4)$-AOL	DFT	1.334	0.976	2.657	1659	3665	2.9[b]	0.12
	DFT-D	1.348	0.980	2.570	1605	3605	1.2[b]	0.77
$p(2 \times 2)$-AOL	DFT	1.339	0.984	3.491	1632	3490	15.1[b]	0.14
	DFT-D	1.356	0.990	3.399	1570	3360	11.3[b]	0.88
$p(5 \times 3)$-2AOL	DFT	1.335	0.985	3.354	1648	3479	17.2[b]	0.25
	DFT-D	1.337	0.994	2.664	1644	3320	5.3[b]	
		1.345	0.993	3.204	1606	3238	14.9[b]	0.91
		1.350	0.998	2.480	1598	3340	5.6[b]	
$p(4 \times 2)$-2AOL	DFT	1.336	0.985	3.413	1645	3487	17.4[b]	0.24
		1.335	0.989	2.874	1651	3399	1.7[a]	
		1.341	0.993	3.199	1619	3334	17.0[b]	0.89
		1.339	0.998	2.515	1639	3233	15.0[b]	

[a] Tilted away from the surface.
[b] Tilted towards the surface.

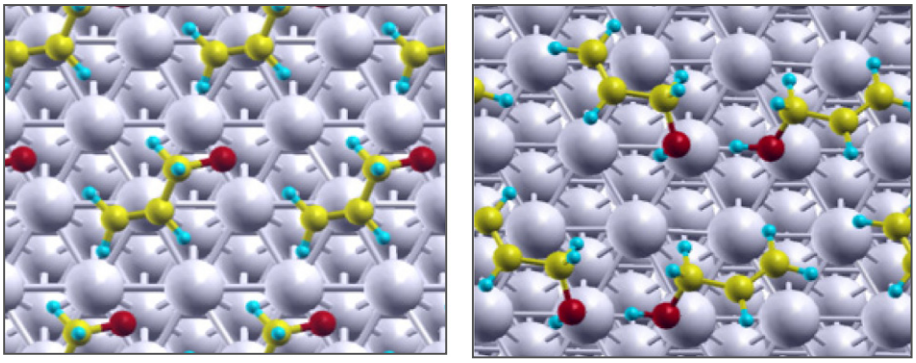

Fig. 5. Top views of the DFT-D optimized geometry of the network of adsorbed allyl alcohol on Ag(111) at the high coverage represented by the $p(2 \times 2)$ (left) and supercells (right).

essentially the same value of E_{ads} but the contributions are very different. Thus, in structure I the molecules in the adsorbed dimer are oriented in such a way that the interaction between them is maximized, the interaction with the surface becoming relatively weak. On the contrary, in structure II with both molecules nearly parallel to the surface, the situation is exactly the opposite.

In the case of AOL adsorption it is interesting to highlight the different contributions observed for the head-to-head orientations as represented in the $p(5 \times 3)$ and $p(4 \times 2)$ supercells. Here, the already mentioned similar E_{ads} values for surface isolated dimers and interacting dimers indicate that the net interacting energy among dimers should be negligible. However, from the values of Table 4 we can note that for the high coverage regime the E_{a-a} energy is higher to the detriment of the E_{a-s} contribution although the difference in the different contributions is quite small. Nevertheless, the present results indicate that the interplay between adsorbate–surface and adsorbate–adsorbate interactions is quite subtle and without the help of accurate theoretical calculations predictions appear to be difficult to make.

3. Conclusions

The interaction of acrolein and allyl alcohol with the Ag(111) surface has been studied by means of periodic density functional theory based calculations neglecting (DFT) or including explicitly (DFT-D and optB86b approaches) dispersion terms. Different coverage values have been explored by suitable choice of supercells which cover different physical situations going from isolated adsorbed molecules to isolated dimers, interacting dimers or ordered overlayers with different types of adsorbate–adsorbate interactions depending on the relative orientation of the adsorbed molecules. For the low coverage situation, both DFT-D and optB86b predict similar values of the adsorption energy of acrolein which are much larger than those predicted by PBE indicating the importance of the dispersion terms in the interaction between this molecule and the metal surface. However, the molecular structure of the adsorbed molecule predicted by DFT-D and optB86b approaches is quite different, the latter being in disagreement with experiments indicating the difficulty to describe van der Waals interactions with non empirical functionals.

In general, the inclusion of the dispersion terms largely affects the calculated values of the adsorption energy and also the distance between the adsorbed molecule and the metallic surface and much less the adsorbate–adsorbate interactions which is not surprising in the view of their essentially electrostatic character. Noticeably, the most stable structure predicted by DFT and DFT-D for both acrolein and allyl alcohol is the same which goes on the line of previous experience indicating that relative energies are usually well represented by DFT.

The present calculations evidence that upon increasing coverage, acrolein tends to form preferentially compact networks in a head-to-tail manner dominated by both adsorbate–surface and adsorbate–adsorbate interactions. However, in the case of allyl alcohol the situation is slightly different with isolated adsorbed dimers and complex networks of adsorbed molecules, in not obvious conformations, having similar stability.

The presence of dimers and of adsorbed overlayers should be taken into account when analyzing the experimental data corresponding either to single crystal studies or to model catalysts.

Table 4
Adsorption energy (E_{ads}) of acrolein (ACR) and ally alcohol (AOL) on Ag(111) for various coverage values corresponding to different ordered superstructures and its decomposition into surface–adsorbate (E_{s-a}) and adsorbate–adsorbate (E_{a-a}) interactions as predicted by DFT and DFT-D calculations. All values are in eV.

	DFT			DFT-D		
	E_{ads}	E_{s-a}	E_{a-a}	E_{ads}	E_{s-a}	E_{a-a}
Acrolein						
$p(4 \times 4)$-ACR	0.06	0.05	0.01	0.61	0.63	−0.02
$p(2 \times 2)$-ACR	0.17	0.00	0.17	0.89	0.74	0.15
$p(5 \times 3)$-2ACR	0.10	0.04	0.06	0.66	0.58	0.08
$p(4 \times 2)$-2ACR (I)	0.15	0.08	0.07	0.62	0.49	0.13
$p(4 \times 2)$-2ACR (II)				0.63	0.56	0.07
Allyl alcohol						
$p(4 \times 4)$-AOL	0.12	0.19	−0.07	0.77	0.88	−0.11
$p(2 \times 2)$-AOL	0.14	0.08	0.06	0.88	0.85	0.03
$p(5 \times 3)$-2AOL	0.25	0.16	0.09	0.91	0.84	0.07
$p(4 \times 2)$-2AOL	0.24	0.10	0.14	0.89	0.71	0.18

Acknowledgments

Financial support has been provided by the Spanish MICINN FIS2008-02238 and MINECO CTQ2012-30751 grants and in part by Generalitat de Catalunya 2009SGR1041 and XRQTC grants. R.M.F. and M.M.B. acknowledge the financial support of CONICET of Argentina and F.I. acknowledges additional support through the 2009 ICREA Academia award for excellence in research.

Appendix A. Supplementary data

Supplementary data to this article can be found online at http://dx.doi.org/10.1016/j.susc.2013.07.005.

References

[1] P. Gallezot, D. Richard, Catal. Rev. Sci. Eng. 40 (1998) 81.
[2] P. Claus, Top. Catal. 5 (1998) 51.
[3] K. Brandt, M.E. Chiu, D.J. Watson, M.S. Tikhov, R.M. Lambert, J. Am. Chem. Soc. 131 (2009) 17286.
[4] H. Wei, C. Gomez, J. Liu, N. Guo, T. Wub, R. Lobo-Lapidus, C.L. Marshall, J.T. Miller, R.J. Meyer, J. Catal. 298 (2013) 18.

[5] R. Ferullo, M.M. Branda, F. Illas, J. Phys. Chem. Lett. 1 (2010) 2546.
[6] J. Shen, K. Muthukumar, H.O. Jeschke, R. Valentí, New J. Phys. 14 (2012) 073040.
[7] M. Mura, N. Martsinovich, L. Kantorovich, Nanotech. 19 (2008) 465704.
[8] K. Toyoda, I. Hamada, K. Lee, S. Yanagisawa, Y. Morikawa, J. Phys. Chem. C 115 (2011) 5767.
[9] T.J. Lawton, J. Carrasco, A.E. Baber, A. Michaelides, E.C.H. Sykes, Phys. Chem. Chem. Phys. 14 (2012) 11846.
[10] K. Toyoda, Y. Nakano, I. Hamada, K. Lee, S. Yanagisawa, Y. Morikawa, Surf. Sci. 603 (2009) 2912.
[11] W. Reckien, B. Kirchner, F. Janetzko, T. Bredow, J. Phys. Chem. C 113 (2009) 10541.
[12] K. Tonigolg, A. Gross, J. Chem. Phys. 132 (2010) 224701.
[13] J. Klimeš, A. Michaelides, J. Chem. Phys. 137 (2012) 120901.
[14] F. Ortmann, F. Bechstedt, W.G. Schmidt, Phys. Rev. B 73 (2006) 205101.
[15] S. Grimme, J. Comput. Chem. 27 (2006) 1787.
[16] A. Tkatchenko, M. Scheffler, Phys. Rev. Lett. 102 (2009) 073005.
[17] M. Dion, H. Rydberg, E. Schröder, D.C. Langreth, B.I. Lundqvist, Phys. Rev. Lett. 92 (2004) 246401.
[18] K. Lee, E.D. Murray, L. Kong, B.I. Lundqvist, D.C. Langreth, Phys. Rev. B 82 (2010) 081101.
[19] J. Klimeš, D.R. Bowler, A. Michaelides, J. Phys. Condens. Matter 22 (2012) 022201.
[20] J. Klimeš, D.R. Bowler, A. Michaelides, Phys. Rev. B 83 (2011) 195131.
[21] J.P. Prates-Ramalho, J.R.B. Gomes, F. Illas, RSC Advances (2013), http://dx.doi.org/10.1039/C3RA40713F, (in press).
[22] P. Janthon, F. Viñes, S. Kozlov, J. Limtrakul, F. Illas, J. Chem. Phys. 138 (2013) 1, (244701).
[23] D. Loffreda, Y. Jugnet, F. Delbecq, J.C. Bertolini, P. Sautet, J. Phys. Chem. B 108 (2004) 9085.
[24] M.E. Chiu, G. Kyriakou, F.J. Williams, D.J. Watson, M.S. Tikhov, R.M. Lambert, Chem. Comm. (2006) 1283.
[25] M.E. Chiu, D.J. Watson, G. Kyriakou, M.S. Tikhov, R.M. Lambert, Angew. Chem. Int. Ed. 45 (2006) 7530.
[26] M. Boronat, M. May, F. Illas, Surf. Sci. 602 (2008) 3284.
[27] Z. Li, Z.X. Chen, X. He, G.J. Kang, J. Chem. Phys. 132 (2010) 184702.
[28] J.P. Perdew, J.A. Chevary, S.H. Vosko, K.A. Jackson, Phys. Rev. B 46 (1992) 6671.
[29] J.P. Perdew, Y. Wang, Phys. Rev. B 45 (1992) 13244.
[30] J.L.C. Fajin, F. Illas, J.R.B. Gomes, J. Chem. Phys. 130 (2009) 224702.
[31] P. Janthon, S.M. Kozlov, F. Viñes, J. Limtrakul, F. Illas, J. Chem. Theory and Comput. 9 (3) (2013) 1631.
[32] P.E. Blöchl, Phys. Rev. B 50 (1994) 17953.
[33] H.J. Monkhorst, J.D. Pack, Phys. Rev. B 13 (1976) 5188.
[34] G. Kresse, J. Furthmüller, J. Comput. Mater. Sci. 6 (1996) 15.
[35] G. Kresse, J. Furthmüller, Phys. Rev. B 54 (1996) 11169.
[36] G. Kresse, J. Hafner, Phys. Rev. B 47 (1993) 558.
[37] S. Linic, M.A. Barteau, J. Am. Chem. Soc. 125 (2003) 4034.
[38] S. Linic, H. Piao, K. Adib, M.A. Barteau, Angew. Chem. Int. Ed. 43 (2004) 2918.
[39] M.-L. Bocquet, A. Michaelides, D. Loffreda, P. Sautet, A. Alavi, D.A. King, J. Am. Chem. Soc. 125 (2003) 5620.
[40] D. Torres, N. López, F. Illas, R.M. Lambert, J. Am. Chem. Soc. 127 (2005) 10774.
[41] E.A. Soares, G.S. Leatherman, R.D. Diehl, M.A. Van Hove, Surf. Sci. 468 (2000) 129.
[42] L.E. Fleck, Z.C. Ying, M. Feehery, H.L. Dai, Surf. Sci. 296 (1993) 400.
[43] H.G. Jenniskens, P.W.F. Dorlandt, M.F. Kadodwala, A.W. Kleyn, Surf. Sci. 357–358 (1996) 624.
[44] R. Wagner, J. Fine, J.W. Simmons, J.H. Goldstein, J. Chem. Phys. 26 (1957) 634.
[45] B.D. Kay, K.R. Lykke, J.R. Creighton, S.J. Ward, J. Chem. Phys. 91 (1989) 5120.
[46] J.R. Durig, A. Ganguly, A.M. El Defrawy, C. Zeng, H.M. Badawi, W.A. Herrebout, B.J. van der Veken, G.A. Guirgis, T.K. Gounev, J. Molec. Struct. 922 (2009) 114.
[47] A. Narasimha Murty, R.F. Curl, J. Chem. Phys. 46 (1967) 4176.